SOCIETY FOR SCIENCE AND EDUCATION UNITED KINGDOM

JBEMi JOURNAL OF BIOMEDICAL ENGINEERING AND MEDICAL IMAGING

ISSN: 2055-1266
VOLUME 6 ISSUE 3

Deep Learning in Retinal Image Analysis: A Review

Adewale Ayuba and Tunde King
Obafemi Awolowo University, Osun, Ile Ife, Nigeria
tunde.king@gmail.com

ABSTRACT

Retinal image analysis holds an imperative position for the identification and classification of retinal diseases such as Diabetic Retinopathy, Hypertensive Retinopathy, Glacuma, Age Related Macular Degeneration, Retinal Detachment, and other retinal disease. Automated identification of retinal diseases is a big step towards early diagnosis and prevention of exacerbation of the disease. A number of state-of-the-art methods have been developed in the past that helped in the automatic segmentation and identification of retinal landmarks and pathology. However, the current unprecedented advancements in deep learning and modern imaging modalities in ophthalmology have opened a whole new arena for researchers. This paper is a review of deep learning techniques applied to 2-D fundus and 3D-OCT retinal images for automated identification of retinal landmarks, pathology, and disease classification. The methodologies are analyzed in terms of sensitivity, specificity, Area under ROC curve, accuracy, and F score on publically available datasets which include DRIVE, STARE, CHASE-DB1, DRiDB, NIH AREDS, ARIA, MESSIDOR-2, E-OPTHA, EyePACS-1 DIARETDB and OCT image datasets.

Keywords— Retinal Imaging, Retinal Image Analysis, Computer aided diagnosis, Systemic Review

1 Introduction

Automatic classification of ophthalmologic and cardiovascular diseases using retinal images in increasingly used in diagnostics. Earlier techniques involved manual segmentation and deniliation of retinal anatomical structures followed by morphometric analysis, which was time-consuming, subjective, and need domain expertise and skill [1]. In contrast, computer-assisted detection of retinal anatomical structures is cost-effective and objective [2]. Development of screening systems are helpful in early diagnosis and real time classification of retinal diseases which includes Diabetic Retinopathy [3], Age Related Macular Degeneration [4], Macular Edema[5, 6], Retinoblastoma, Retinal Detachment [7], and Retinitis Pigmentosa [8].

All these state-of-the-art methods required manual feature designing through SURF, SIFT, and HOG feature descriptors [9-11]. The specific domain knowledge about retinal imaging is mandatory requirement for generating this kind of meaningful hand crafted feature extraction [12]. In geneal, the generated hand crafted features are not generalizable across the datasets [13]. Recent advancements in visual recognition via deep learning motivated the researchers to use convolutional neural networks for recognizing varius retinal landmarks. Convolutional Neual Netorks can learnd the intricate retinal features automatically. The supervised and unsupervised multi-layer Deep Neural Networks (DNN) allow

DOI: 10.14738/jbemi.63.9492
Publication Date: 29th June 2019
URL: http://dx.doi.org/10.14738/jbemi. 63.9492

generalized high level feature extraction from raw data image [12]. Whereas, retinal image analysis based on deep learning has outperformed the traditional methods both for 2-D fundus images and 3-D OCT images.

Abràmoff et al., [2] have discussed retinal imaging and retinal image analysis based on 2-D fundus and 3-D OCT images. However, this review encompasses only conventional techniques for retinal deformity detection. Moreover there are many other reviews and survey papers which cover the domains of retinal landmark detection, retinal pathology segmentation [7, 14] , and retinal disease classification [1, 15]. The major contribution of this paper lies in the fact that there is no existing survey paper which covers deep learning based retinal image analysis. This work is a review of 2-D fundus and 3-D OCT retinal images' analysis using modern deep learning techniques for automated identification of retinal landmarks, pathology, and disease classification. We have analyzed and compared algorithms on the basis of a diverse set of performance metrics which include: sensitivity, specificity, area under ROC curve, accuracy, F-score, positive predictive value, and Kappa measure. The objective of this work is to summarize the current progress made in the field of ophthalmology using deep learning techniques.

1.1 Methodology of literature Search

A systematic methodology has been developed for searching literature for this study. This systematic methodology includes the following stages:

- Defining research problem
- Finding pertinent articles that satisfy the pre-set inclusion criteria
- Extracting relevant data from articles
- Assessment of quality of extracted data

All the literature that has been reviewed in this survey was retrieved by conducting iterative and exhaustive searches on following databases:

1. IEEE Xplore Digital Library, (http://ieeexplore.ieee.org)
2. Springer Link, (http://link.springer.com/)
3. ScienceDirect, (http://www.sciencedirect.com/)
4. American academy of Ophthalmology, (http://www.aaojournal.org/)
5. The JAMA Network, (http://jamanetwork.com/journals/jama)
6. Investigative Ophthalmology and Visual Science, (http://iovs.arvojournals.org/)

All journal papers as well as conference papers that have been published in the proceeding of above mentioned bibliographic databases have been included in this review. Keywords that have been used to perform the search are: deep learning, deep neural network, convolutional neural network, auto-encoder, sparse stacked auto-encoder, de-noised sparse auto-encoder, softmax, random forest, rectified linear unit, hidden layers, diabetic retinopathy, exudate detection, exudate segmentation, micro-aneurysms detection, micro-aneurysms segmentation, OD localization, fovea localization, retinal blood vessel segmentation, age related macular degeneration, automated screening, retinal disease classification.

1.2 Inclusion Criteria

"Application of deep learning for retinal image analysis" has been set as the cue statement for literature search. Abstracts and titles of all collected articles are checked against the research cue and only those articles are selected which provide deep learning based algorithms for segmentation of retinal anatomical structures and retinal disease classification. All the relevant content up till July, 2017 has been included in this survey.

1.3 Exclusion Criteria

The main focus of this survey is to review deep learning based techniques for retinal image analysis. Therefore, the articles whose algorithms are not based on deep learning concepts are excluded from this survey. Moreover, the articles from impact factor journals and reputed conferences have been selected in this review. We have avoided inclusion of such papers which were published in local journals and conferences.

1.4 Selection of papers

Articles were selected through vigilant scrutiny of inclusion and exclusion criteria. Selected articles were downloaded in pdf format and saved. The nomenclature used for saving selected papers depict publishing year, journal name/conference name, publisher, main author name, and title. This type of nomenclature helped in indexing the articles and resulted in efficient retrieval in accordance with queries. Citations of all the articles have also been downloaded and saved in EndNote library.

2 Diagnostic analysis and Screening of retinal images

Retinal image analysis allows detection and diagnosis of many diseases originating in brain, eye or cardiovascular system, as these diseases manifest themselves in retina.

2.1 Retinal imaging modalities

Precise imaging of retinal tissues and brain tissues is very important for the diagnosis and treatment of retinal impairments. Czech scientist Jan Evangelista Purkyně [16] invented principles of ophthalmoscope in 1823 as a first attempt towards direct inspection of retina. Since then many imaging modalities have been developed for non-destructive visualization of retinal anatomical structures. Fundus photography has been found to be effective for early screening and diagnosis of three most important causes of blindness in industrialized world [17]. The 2-D representation of retinal world obtained by preliminary fundus cameras lacked the ability to apprehend depth during examination of fundus image which lead to inaccurate diagnosis of certain retinal pathology (e.g. cotton wool spots). Tomography based imaging has resolved this problem. Optical coherence tomography (OCT) has now been successfully employed to develop 3-D view of retina [18].

2.1.1 Fundus photography

The process of obtaining a 2-D representation of 3-D ocular fundus through projection of reflected light on to an imaging plane is termed as fundus photography. Fundus photography, mydriatic or non mydriatic, involves use of a low power intricate microscope with an attached camera for imaging the interior surface of the eye which includes retina, OD, retinal vasculature, posterior pole, and macula. Digital Imaging of inner lining of eye surface through fundus photography follows the same footings as those of conventional image capturing except that instead of a photographic film, digital cameras have sensors (charge coupled

device or complementary metal oxide semiconductor active pixel). Each sensor converts light signal into electric signal and result is stored in the form of a single pixel. The resolution of image can be increased by increasing number of sensors.

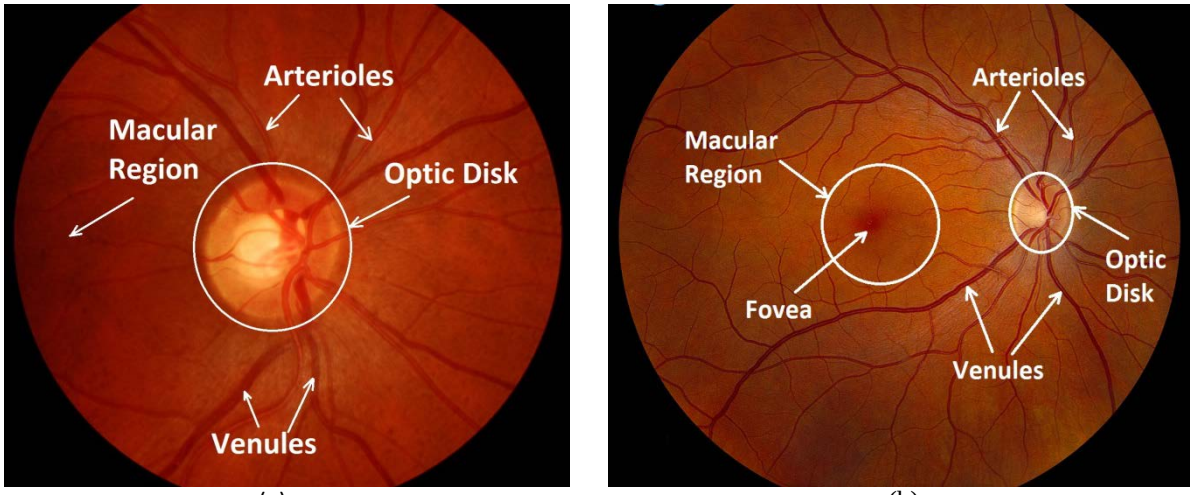

(a) (b)

Figure 1 Retinal fundus images (a) OD centered (b) Macula centered

Advancements in the models of fundus photography have been witnessed since the last century [2]. The modern fundus photography includes the following imaging modalities:

Color fundus photography modifies spectral range of illumination source through the use of contrast filters (red, blue, and green filters). This variability in spectral range of illuminating source enhances visibility of several ocular structures. For instance, blue color improves perceptibility of anterior retinal layers, which appear transparent in the presence of white light. Moreover, blood vessels and retinal pigments absorb blue light resulting in a dark background which enhances specular reflections and scattering in anterior fundus layers. On the other hand, green light provides the best global retinal view because the retinal pigmentations reflect green light more than blue light providing excellent contrast. Hence, green filter is employed in color fundus photography for improved visualization of retinal vasculature, drusen, exudates, and hemorrhages. Retinal pigments, blood vessels and optic nerve appear almost featureless in red light and overall contrast of retinal images is reduced. Hence, red light is only used for revealing the choroidal pattern, pigmentary disturbances, choroidal ruptures, choroidal naevi, and choroidal melanomas [19].

Red free photography is the process of retinal image acquisition in the presence of an illumination source with a specific color filter to block red light, usually green filter is used for this purpose. This kind of fundus photography is effective in viewing retinal blood vessels, hemorrhages, pale lesions (exudates and drusen), epiretinal membranes, and retinal nerve fiber layer defects [20].

Stereo fundus photography [21] helps in documenting the retinal structures because of its increased depth resolution feature. This type of photography involves simultaneous or sequential visualization of retina through two cameras with different angles of observation insuring least stress to the patient and it is viable for diagnosis of macular edema (ME) and sub retinal neovascularization.

Hyper-spectral imaging allows efficient visualization of retinal lesions with high spatial and spectral resolution. The illumination source has multiple wavelength bands and their reflection is recorded in the form of hyper-spectrali image intensities. This type of imaging modality is feasible for retinal blood oxygen saturation analysis (oximetry) [22] through likening of spectral absorptions by retinal arteries, veins, and surrounding regions. Hyper-spectral imaging is appropriate for screening and diagnosis of diseases such as: diabetes, age related macular degeneration, and glaucoma [23].

Scanning Laser Ophthalmoscopy (SLO) [24] uses a focused laser beam to illuminate the retinal fundus and provides retinal images with high spatial sensitivity. It is helpful in diagnosis of retinal disorders such as macular degeneration and glaucoma.

Adaptive Optics SLO [25] utilizes SLO and enhances the results by removing aberrations from retinal images through adaptive optics. The retinal images obtained by adaptive SLO are sharper than those obtained by SLO.

Angiography is the process of injecting fluorescent dye in retinal blood vessels and projection of emitted photons from the dye on to an imaging plane. The fluorescent dye, which is injected in circulation, is sensitive to the light reaching it i.e. the fluorescence is different for different wavelengths of light. This chameleon behavior of fluorescent dye makes angiography an apposite imaging modality for inspection of retinal blood circulation [26].

1. ***Sodium Fluorescein Angiography (FAG)*** is a variation of angiography. However, the fluorescent dye injected in retinal blood circulation is sodium. When the retinal blood vessels and neighboring retinal tissues are illuminated with blue light (490nm wavelength), the dye fluoresces yellow light (530nm wavelength). It is helpful in documenting the retinal manifestaions of cystoid macular oedema and diabetic retinopathy [26].
2. ***Indocyanine Green Angiography (ICG)*** is another variant of angiography which employs indocyanine as fluorescence agent. The injected indocyanine glows only in infrared spectrum thereby making the blood, fluids, and choroidal pigments, present in posterior part of eye, transparent for the observer. This behavior makes it appropriate for diagnostic analysis of deep choroidal disorders such as choroidal neovascularization, abnormal vessels supplying ocular tumors, and hyperpermeable vessels leading to central serous chorioretinopathy [27].

A diverse set of datasets based on retinal fundus photography, from different ethnicities, has been developed. Some of them are publically available while others can be obtained on demand. A brief overview of these datasets is presented in Table 1.

Table 1 Specifications of 2-D fundus Retinal Image Datasets

Sr.	Dataset	Source	Camera Specs.	Field of view (FOV)	Image format	Number of groups	Image size(pixels)	Number of Images	Ground Truth	Availability
1	DRIVE [28]	DR screening test held in Netherlands	Canon CR5 non-mydriatic 3-CCD camera	45^0	JPEG compressed	1	768 × 584	40	Blood Vessel demarcation	Public
2	STARE [29]	Shiley Eye Center at the University of California, San Diego, Veterans Administration Medical Center in San Diego.	TopCon TRV-50 fundus camera	35^0	-	1	605x700	20	Blood Vessel demarcation	Public
3	ARIA [30]	St. Paul's Eye Unit, Royal Liverpool University Hospital Trust, Liverpool, UK and the Department of Ophthalmology, Clinical Sciences, University of Liverpool, Liverpool, UK	Zeiss FF450+ fundus camera	50^0	Uncompressed TIFF	3	768x576	92 59 61	Trace of blood vessels, the optic disc and fovea location	Public
4	CHASE-DB1 [31]	Child Heart and Health Study in England (CHASE),	Nidek NM-200-D	30^0	TIFF	1	1280x960	28	Blood Vessel demarcation	Public
5	DIARETDB0	Captured under IMAGERET project	Several digital fundus cameras	50^0	PNG	1	1500x1152	130	Each image is marked as having any red small dots, hemorrhages, hard exudates, soft exudates, neovascularization or not	Public
6	DIARETDB1	Captured under IMAGERET project	Several digital fundus cameras	50^0	PNG	1	1500x1152	89	Demarcation of red small dots, hemorrhages, hard exudates, and soft exudates	Public
7				45^0	TIFF	3	1440 x 960	1748		On demand

	MESSIDOR-2 [32], [33]	LaTIM laboratory and the Messidor program partners	TopCon TR NW 6 3CCD fundus camera				2240 x 1488 2304 x 1536			
8	E-Ophtha EX [34]	ANR-TECSAN-TELEOPHTA project	-	-	JPEG	1	2544x1696 2048x1360 1440x960	82	Exudates marked	Public
	E-Ophtha MA [34]	ANR-TECSAN-TELEOPHTA project	-	-	JPEG	1	2544x169 1440x960	381	Micro-aneurysms marked	Public
9	NIH AREDS	Project funded by NIH	-	-		1		5600		Public
10	DriDB [35]	university hospital in Zagreb	Zeiss VISUCAM 200 fundus camera	45^0	Uncompressed BMP	1	720 x 576	50	location of OD, blood vessels, hard exudates, soft exudates, dot and blot hemorrhages, and neovascularization	On Demand
11	EYE-PACS1	Captured during regular screening of DR affected patients under EYEPACS program	Canon CR1/DGi/CR2, Centervue DRS, and Topcon NW camera	45^0	JPEG	1	Varying sizes	9963	Each image marked as having: No DR, Mild, Moderate, Severe or Proliferative DR	Public

2.1.2 3-D Optical coherence tomography

Optical coherence tomography (OCT)[36] is a widely accepted noninvasive imaging modality among ophthalmologists. This technique captures 3D cross-sectional maps of retina by utilizing the principle of interferometry and confocal microscopy. Accuracy of 3D OCT images is usually 10 to 15 microns. Depending on the light source used, resolution of images can be improved. The illumination source with large wavelength is preferable because it provides efficient scattering of light in retinal cross-section. These images are efficient in diagnosis of macular pucker, vitreomacular traction, macular hole. However, OCT has recently been regarded as a new standard for detection of diabetic macular edema. The advancement in technologies has made OCT capable of generating angiograms for assessment of retinal vasculature.

2.2 Retinal Anatomical structures

Human eye, which is mostly a hollow organ, is internally lined by light sensitive tissues collectively named as the retina. The posterior pole of the eye is tightly knit with neuronal cells, photoreceptor cells, and glial cell. Rods, cones and ganglion cells are three types of photoreceptor cells. The optic nerve fibers originate from nerve fiber layers which emanate from axons of ganglion cells. The ocular structures focus the image on retina and nerve fibers transfer the information to brain in the form of electrical signals which then

interprets the received signals as visual images. Optic nerve head or OD, oval in shape, serves as the exit point for nerve fibers and is located 4.5 mm to 5 mm nasal to the center of retina as depicted in Figure 1. The maximum resolving power of the eye comes from the anatomical center of eye i.e. macula. Fovea and foveola are present in the macular region and both of them contain a large number of photoreceptors (cones) making them specialized retinal region for high acuity vision [37]. Visual capacity of human brain is primarily dependent on visual input from macula but progressive damage to macula results in inculcation of diseases like macular degeneration or in severe cases can create macular hole bursting the blood vessels coursing towards macula.

Ophthalmic artery provides the circulation to the retina. Retinal blood vessels exist in the form a network of arterioles and venules which circulate the whole retinal region. Due to nonfenestration of the vascular endothelium a blood-retina barrier is maintained by retinal blood vessels. Micro-aneurysms and hemorrhages are produced as a result of damage to this blood-retinal barrier. Moreover, out pouching of retinal blood vessels appear as neovascularization disturbing their morphology. Various systemic and retinal diseases manifest themselves in the form of variation in retinal blood vessels' features.

2.3 Disease Manifestations as Retinal Impairments

Analysis of retinal morphology provides an insight to general health state of entire human body as many systemic and retinal diseases manifest themselves as ocular structures' impairments[14, 38, 39]. Following paragraphs provide a compact overview of such diseases.

2.3.1 Diabetic Retinopathy

Diabetes mellitus (DM) is a disease caused by fluctuating levels of glycemia (hypoglycemia, hyperglycemia). Repercussions of DM can emanate as asymptomatic development of diabetic retinopathy (damage to the eyes), diabetic nephropathy (damage to kidneys), and diabetic neuropathy (damage to nerve) [40]. The most prevalent consequence of DM is diabetic retinopathy. Despite the use of intensive glycemic control therapy DR remains a vision threatening complication of diabetes. Severe symptoms of DR include development of micro-aneurysms, neovascularization, hemorrhages, cotton wool spots, and exudates in the retinal region. Extreme progression of polygenic disease puts the patient's eyesight at stake [41]. Pathogenesis like capillary closure and dysfunction of blood-retina barrier are the main anatomical changes in retina that lead to DR. Their brief detail is mentioned in the following sections.

2.3.1.1 Retinal Vessel closure

Many retinal disorders stem from obliteration of retinal capillaries such as neovascularization is reported to be preceded by nonperfusion and closure of small retinal blood vessels[38, 42, 43]. Retinal vessel closure instigates the development of neovascularization, micro-aneurysms, cotton wool spots, and hemorrhages.

Neovascularization: Retinal blood vessel closure leads to limited supply of oxygen to retinal regions corresponding to these vessels. This condition is often termed as retinal ischemia [44]. The vascular endothelial growth tries to compensate the decreased oxygen supply resulting in the formation of weak small blood vessels on the surface of retina thereby leading to vision loss.

Micro-aneurysms: Limited oxygen supply results in unusual dilation of retinal capillaries. These bulgings of capillary endothelial linings often appear in the form of small sac like structures named as micro-

aneurysms. The fragility of capillary walls is considered to be the main reason behind development of micro-aneurysms [45]. They appear as small red dots in retinal images as depicted in Figure 2.

Cotton wool spots: Oxygen supply to certain retinal areas may completely close off due to blockage in arterioles. Consequently large regions of retina become completely deprived of oxygen and result in emanation of fluffy white patches identified as cotton wool spots or soft exudates [45].

Hemorrhages: The blockade in arterioles may instigate a pressure build up within the vessels. Significant amount of pressure could burst the vessels and result in origination of hemorrhages [45] as shown in Figure 2.

2.3.1.2 Mutilation of blood-retina barrier

Retinal blood vessels are permeable i.e. they allow motion of fluids through their walls. In DR, the retinal vessels become fenestrated and abnormal leakage of blood cells, proteins, water and other large molecules starts.

Hard Exudates: They appear as a consequence of leakage of fats and proteins along with water from abnormally permeable walls of retinal vessels. Mostly hard exudates appear on the outer layer of retina individually, in the form of patches, or surrounding micro-aneurysms in the form of a crescent. They appear as yellowish, waxy, and glistering structures in retinal images as presented in Figure 2.

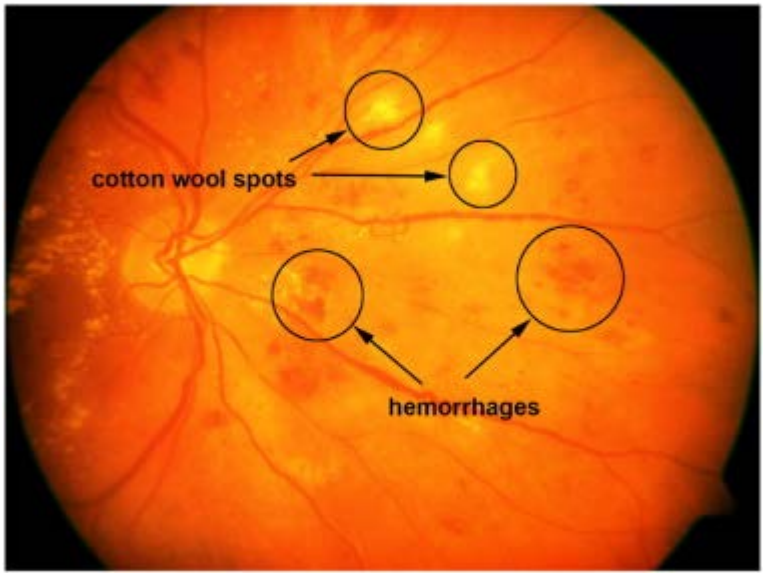

Figure 2 (a) A sample retinal image showing pathological structures

The central region of retina is macular region and is responsible for high acuity vision. Macular edema (ME) is a consequence of retinal thickening near macula and fenestration of retinal blood vessels. The anomalous vasopermeability allows abnormal flow of large molecules like water, blood cells, lipids, and proteins through retinal vascular walls. Accumulation of such fluids in the macular region results in the development of pigments such as exudates leading to ME. Treatment of ME is only recommended when the pigmentations develop at the center of macula i.e. fovea. This condition is termed as clinically significant macular edema (CSME). CSME is actually defined as presence of hard exudates within 500µm of the macular or retinal thickening within 500µm of the macular region [46]. Prolonged and asymptotic

DM results in the origination of diabetic macular edema preceded by proliferative and non-proliferative DR [47].

Severity levels of DR have been graded based on the variants of pathology present in retina. A brief detail about grading levels of DR, in accordance with the severity, is presented below:

- ***Proliferative DR (PDR)*** is marked by presence of retinal hemorrhages.
- ***Moderate PDR*** manifests itself in the form of neovascularization and retinal hemorrhages.
- ***Severe PDR*** is indicated by the presence of detachment of retina and neovascularization on iris.
- ***Insignificant non-proliferative PDR (NPDR)*** signs are micro-aneurysms, retinal hemorrhages, and the presence of hard exudates
- ***Significant NPDR*** has similar signs as those of insignificant NPDR with vessel closure.
- ***High Risk NPDR*** depicts itself as retinal hemorrhages and vessel closure.
- ***Moderate ME*** is indicated by hard exudates, origination of Oedema outside fovea region, and thickening of retina.
- ***Severe ME*** manifestations are similar as those of moderate ME except that Oedema develops inside the fovea region.

2.3.2 Age Related Macular Degeneration

For people of age above 50 years, AMD is found to be the chief cause of irreversible vision loss. Presence of age related macular degeneration (AMD) is characterized by excessive presence of drusen, yellow dots, in the macular region of eye. Small number of hard drusen is not regarded as symptoms of AMD because people with age more than 50 years are likely to develop drusens as a normal anatomy of retina. But anomalously large number of drusen can result in mutilation of retinal pigment epithelium [48]. AMD can be classified into the following categories:

Early AMD is marked by the presence of less than 20 medium sized drusen or other abnormal retinal pigments [49].

Intermediate AMD is characterized by the presence of many medium sized drusen, one large druse or geographic atrophy that is away from the center of macula [49].

Advanced non-neovascular AMD (Dry AMD) manifests itself in the form of drusen and geographic atrophy that extends to fovea i.e. the center of macula [49].

Advanced neovascular AMD (Wet AMD) is indicated by presence of exudates, neovascularization, and sequelae of neovascularization [49].

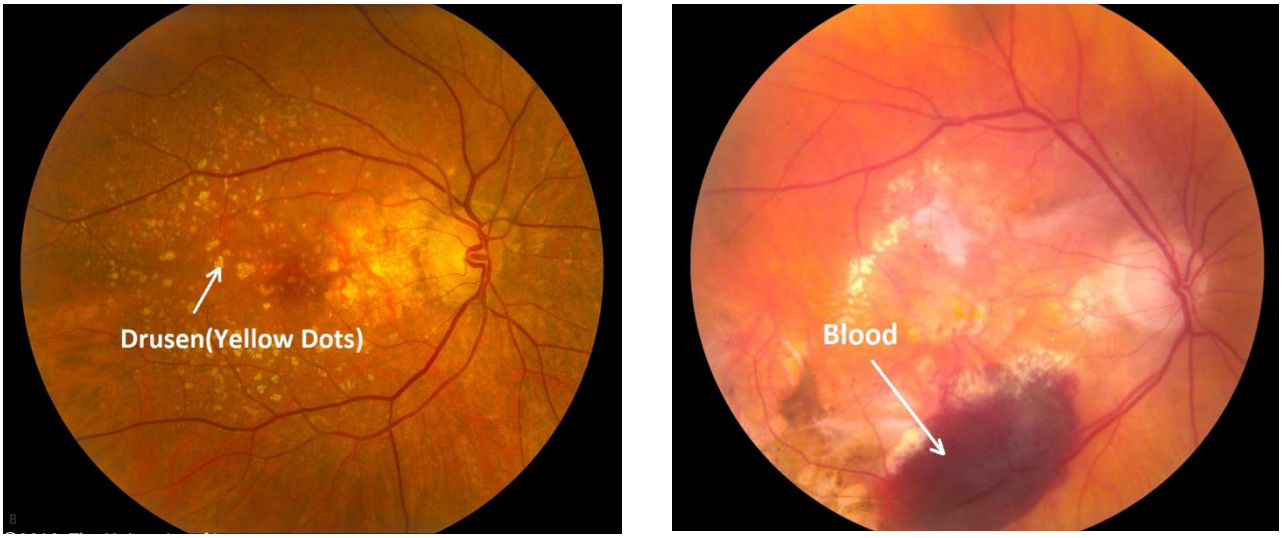

(a) (b)

Figure 3 Retinal image diagnosed (a) with Dry AMD (b) with Wet AMD

2.3.3 Cardiovascular Diseases

Coronary heart disease is directly linked with micro-vascular circulation [50]. Changes in microvasculature, structure and pathology of human circulation can be studied through in vivo examination of retina [51]. Therefore, retinal image analysis provides a window in the health of human heart. Common retinal vascular signs include formation of micro-aneurysms, hemorrhages, arterio-venous nicking, and focal arteriolar narrowing [4]. These signs reflect vascular damage because of hypertension, aging, and other processes. Retinal vascular narrowing is found to be associated with reduced myocardial perfusion measures on cardiac magnetic resonance imaging. Moreover, it has also been found that other retinopathy lesions are linked to coronary artery calcification. These kind of anatomical and pathological reasons suggest that changes in retinal microvasculature can be useful for assessing the coronary heart disease risk stratification [52].

2.3.4 Glaucoma

The second most prevalent cause of permanent vision loss in the developed world is glaucoma. This disease directly damages the optic nerve and the ganglion cells [53]. Optic nerve of glaucoma affected eye shows cupping of optic nerve up to an abnormal amount. Obesity, high blood pressure, migraines, and increased pressure in eye are the factors that instigate glaucoma [54]. Glaucoma is classified as open angle, close angle, and normal tension glaucoma. Open angle glaucoma is the most prevalent type of glaucoma. It grows gradually and is painless but it has the potential of making the patient completely blind if left untreated. However, closed angle glaucoma has the ability to manifest itself slowly or abruptly. Normal tension glaucoma is associated with blood circulation issues in retinal area and other organ perfusion whereas the classic hallmark of intra-occular pressure has no association with this kind of glaucoma. Glaucoma is diagnosed by analysis of intra-ocular pressure, cup to disk ratio [3], retinal vascular morphology [55], optic nerve structure, and anterior chamber angle [56].

2.4 Quantitative Measures for Retinal Image Analysis

An algorithm is considered efficient if its predictions and ground truth stand in close proximity to each other. This proximity can only be tested by the use of some quantitative measures. These quantitative measures also help in evaluating and comparing the capabilities of different algorithms. Sophisticated performance metrics are derived from basic performance measures (true positives, false positives, true negatives, and false negatives). The performance metrics which are used for analysis and comparison of algorithms in this study are recorded in Table 2.

Table 2 Performance Metrics for Retinal Image Analysis

Performance Metric	Description
Sensitivity(SN)	TP/TP+FN
Specificity (SP)	TN/TN+FP
Accuracy (Acc)	TP+TN/FOV pixel point
Positive Predictive Value (PPV)	TP/TP+FP
Negative Predictive Value (NPV)	TN/TN+FN
F-score	SN.PPV/PPV+SN
Kappa	Acc-Accr/1-Accr

3 Deep-Learning

Creation of self-taught and self-thinking machines has remained utter desire of humans since antiquity. With the invention of programmable computers, scientists remained focused towards tackling problems which were intellectually difficult for humans in early days of artificial intelligence. Artificial intelligence has coursed through the following phases before turning the milestone of self-taught machines [57]:

Knowledge based AI: This approach of AI required the programmers to feed the machine with all the details about the problem. Surprisingly the use of knowledge base approach made a number of monotonous tasks easier for machines to solve. Through *knowledge base* approach to artificial intelligence (AI), computers have defeated even the best chess player, Garry Kasparov [58].

Machine Learning: Solving intuitive and subjective problems, such as recognizing voices and contents of an image, proved to be a taxing task for AI. Solution of such intuitive tasks required immense amount of knowledge about the surrounding world and a large database of decision statements. These challenges suggested that instead of hard-coded knowledge, AI systems required to develop self-learning ability from raw data. This concept surfaced as the field of machine learning. Performance of machine learning algorithms was primarily dependent on representation of data provided to them. Maiden machine learning algorithms required manual representation of data in the form of features. The algorithms deduced results on the basis of correlation between features and output. Logistic regression and Naïve Bayes are examples of machine learning algorithms.

Representation Learning: Hand crafting of features for tedious tasks is laborious and time consuming. It may take decades for a community of researchers to devise maximally correlated features for such complex tasks. This problem was tackled by the development of representation learning which is learning of mapping from initial representation of data to an intermediate representation and then back to the original representation. A classic example of representation learning is auto-encoder.

Deep Learning: Many *factors of variation* are associated with learned features in case of representational learning. An example of factors of variation is the different viewing angles with which an image of a car is captured. Concepts of deep learning or experience based learning come handy in solving this crucial problem of representation learning. Hierarchical nature of deep learning techniques allows building of complex concepts out of simpler ones. Quintessential example of deep learning technique is feed forward network termed as multi-layer perceptron (MLP). These techniques are well established in audio recognition, natural language processing, and automatic speech recognition [59].

Benefits of deep learning are achieved through the use of Deep Neural Network (DNN). It is a form of artificial neural network (ANN) in which arrangement of neurons is inspired by neuron disposition of animal visual cortex. DNN provide the following major commendatory advantages:

1. Hierarchical feature extraction i.e. no need of handcrafted features.
2. Limited pre-processing of input images

DNN have three kinds of layers: input layer, hidden layers, and output layer. Each layer has non-linear units known as nodes which help in modeling of complex features. DNN can learn features by following either the supervised learning method or the unsupervised method. A brief introduction of these methods is listed under the following rubrics.

3.1 Supervised Learning

In supervised method DNN is provided with training data along with output labels and network tries to learn labeling using a specified learning method under the supervision of available ground truths. Classification problems are solved using supervised learning approach.

As cortical neurons in animals consider a restricted region of space to generate response, similarly convolutional neural network (CNN) neurons respond to a restricted region of input image known as *receptive field*. This receptive field can be viewed as an image processing filter or kernel. Receptive fields are overlapping, to give an effect of sliding over input image. Response is generated by convolution of receptive field of neuron with weight matrix (generated by individual weights of neurons in same layer). Each node of input layer gets an input image patch, and output is generated for central pixel of patch as shown in Figure 4. Output label maps for all pixels of input image patch can also be generated simultaneously using *structured prediction* method.

Usually CNNs have convolutional layers, pooling layers, and a terminating classification layer. *Pooling layers* are used to reduce dimension of feature vector which further increases computational efficiency of the network as shown in Figure 4c. Softmax, LSVM, multi-class SVM, random forest etc. can serve the purpose of classification layer. CNNs have many variations depending on number of layers, pooling, and classifier. These include LeNet-5, VGG16, and GoogleNet etc.

3.2 Unsupervised Learning

This approach is used for pattern recognition. Unsupervised DNNs also have input layer, hidden layers, and output layer. These layers can be partially or fully connected, we can also have a terminating fully connected classification layer. Unsupervised DNN take input image and compress it, their principle is to reconstruct input image from compressed version of input image. This reconstruction is probabilistic. A number of network variants exist which include: auto-encoders, stacked auto-encoders, stacked de-noised auto-encoders, restricted Boltzman machines etc. Usually noise is added in input images and stacked de-noising auto-encoder is then used to reconstruct original image from compressed noisy image.

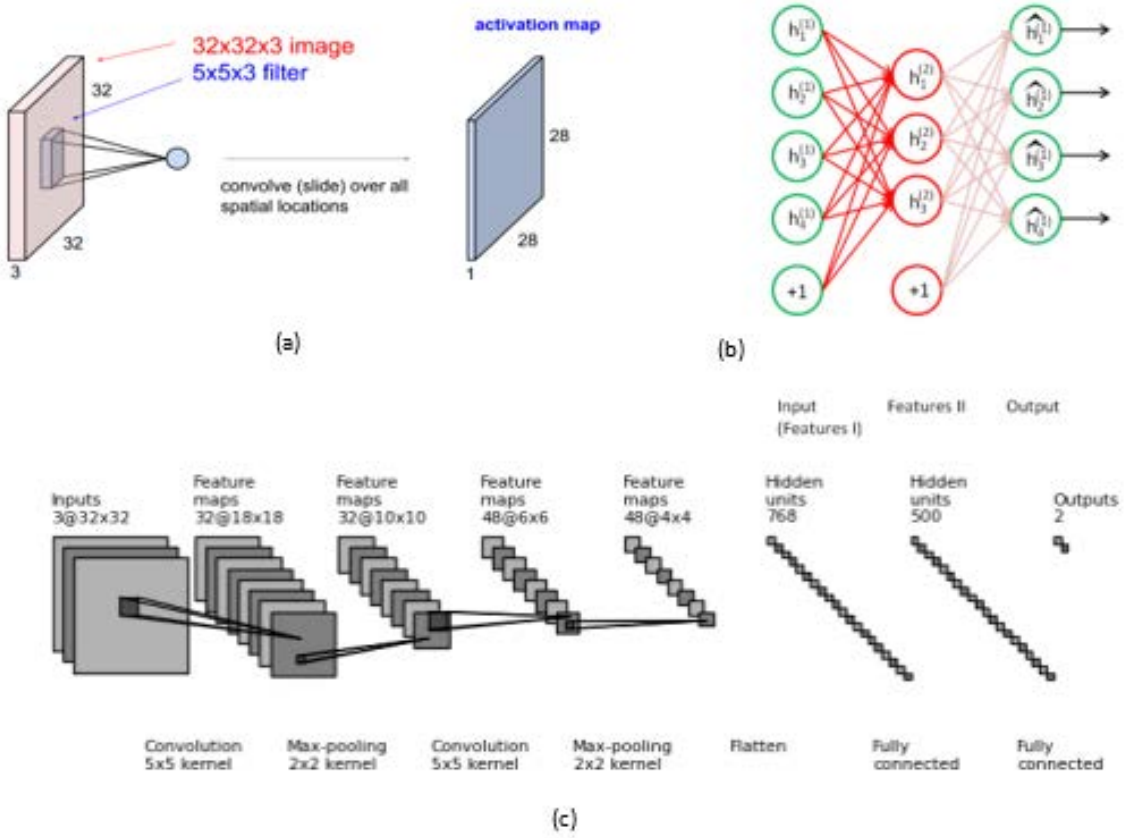

Figure 4 Deep Neural Networks (a) Receptive field of CNN (b) Supervised CNN (c) Structure of CNN

3.1Challenges to Deep Learning

In recent years deep learning techniques have emerged as revolutionary methods which have surpassed the state-of-the-art techniques. The ability of deep networks to exploit simple as well as complex compositional features of data representations is referred to as the reason behind their success. Notwithstanding, there are some issues with deep learning techniques which are yet to be solved.

3.2.1 Lack of real cognizance behind Deep learning techniques

Despite achieving remarkable performance, the real cognizance behind the achievements of deep learning has remained unknown. A small number of efforts have been put forth by researchers to understand how deep networks achieve such exceptionally good results. However, there is a utmost need

to develop a comprehensive theoretical background about tuning and performance assessment strategies of deep networks [60]. The following questions are still unanswered.

i. How to choose features to be extracted?
ii. How to tune parameters of network models?

3.2.2 Difficult training

Training of deep neural network has always remained a difficult task as there are numerous chances that they network may get stuck in local optima. Moreover, training of deep networks is very slow and requires massive computational resources for both medium and large sized data-sets to reach performance of state-of-the-art performance especially in case of offline learning. Once trained the network becomes non-adaptive for new data [60].

4 Learning Methods applied for Retinal Image Analysis

4.1 Healthy and Abnormal Retinal Anatomy Segmentation

4.1.1 Supervised Methods

Supervised Retinal vessel segmentation problem can be broken down into two stages: (i) feature extraction, (ii) classification. Wang *et al.,* [61] have exploited the same approach with CNN as a hierarchical feature extractor. Ensemble Random Forest (RF), which has good generalization ability, is used as classifier. This classifier gives a binary output for each pixel as vessel pixel or background pixel. The green channel of RGB images contains the best retinal vessel and background contrast therefore green channel of images is used in proposed methodology. To reduce the noise and normalize uneven illumination in images Histogram equalization and Gaussian smoothing filter are utilized. Training of network is compute intensive therefore super-pixel based sample selection is done using Simple Linear iterative clustering (LISC). However CNN, which is used as a trainable feature extractor, has alternating convolution and subsampling layers. The network has five layers (classic LeNet5) with one fully connected output layer. Features learned from intermediate subsampling layers and last fully connected layer are fed into three RF classifiers. During training, input nodes of network are supplied with square shaped image patches. Each node's output is a single pixel in activation map. After training of CNN, each RF is trained with learned features extracted from the network. An ensemble classifier with winner-takes-all strategy has been employed after complete training of RFs. DRIVE and STARE datasets are used to test efficacy of proposed method. Table 4 shows average case performance metrics of algorithm for both datasets. Robustness of algorithm is inspected using cross training. Accuracy in case of DRIVE (trained on STARE) is 0.9803 and for STARE (trained on DRIVE) accuracy is 0.9710.

Classification of each pixel as vessel or non-vessel poses two problems: (i) system is not robust to pathology presence and (ii) pixel-pixel training of network is exhaustive. Structured prediction i.e. output label map for all pixels in input image patch instead of a single label for central pixel is more computationally efficient. It makes the system independent of pathology presence. This approach is presented in detail by Fang *et al.,* [62]. Their DNN has five layers with three hidden layers and nodes of hidden layers are twice as those of input layer, network is made wide to make feature extraction effective. To allow learning of complex relationship between cross-modalities, input image patch and output label map, network is made deep. The label map is used to construct probability map which is of the same size

as that of original retinal image. Probability map is enhanced by histogram equalization. The scale space helps in highlighting fine details in image. Enhanced probability map is smoothed with Gaussian kernels of varying standard deviation to get different scale space images. Hessian matrix for each pixel is obtained by computation of second derivatives of distinct scale space images. Coherent pixels are extracted from candidate pixels through non-maxima suppression of determinant of hessian matrix, determinant fine-tunes high curvature points. This approach is more objective and results are not affected by image noise and other unwanted image artifacts. Results are tested on DRIVE dataset and compared with state-of-the-art SIFT and COSFIRE methods. The proposed method has superseded the traditional methods in identification of bifurcation points, extreme curvature and cross-over points.

Table 3 Deep Learning Based Retinal Image Analysis Methods

Algorithm	Year	Photography	Dataset	Focus	Method	Deep Learning Technique	Network Architecture	Classifier	
Maji *et al.,* [63]	2015	Fundus images	DRIVE	Retinal vessel detection	Hybrid	DAE	-	Random Forest	Healthy and Abnormal Retinal Anatomy Segmentation
Wang *et al.,* [61]	2015	Fundus images	DRIVE STARE	Retinal vessel Segmentation	Supervised	CNN	LeNet5	Ensemble Random Forest	
Fang *et al.,* [62]	2015	Fundus images	DRIVE	Retinal vessel detection	Supervised	CNN	5 layers	-	
Melinščak *et al.,* [64]	2015	Fundus images	DRIVE	Retinal vessel detection	Supervised	CNN	2 convolutional layers, 2 max pooling layers, 2 fully connected layers	Softmax	
Fu *et al.,* [65]	2016	Fundus images	DRIVE STARE	Retinal vessel Segmentation	Supervised	CNN	4 convolutional layers with 3 alternating max pooling layers, a side output layer	CRFs	
Fu *et al.,* [66]	2016	Fundus images	DRIVE STARE CHASE-DB1	Retinal vessel Segmentation	Supervised	DeepVessel Network	4 convolutional layers with 3 alternating max pooling layers, a side output layer	RNN	
Liskowski & Krawiec [67]	2016	Fundus images	DRIVE STARE	Retinal vessel Segmentation	Supervised	CNN with structured Prediction	Convolutional layers with max pooling	-	
Li *et al.,* [68]	2016	Fundus images	DRIVE STARE CHASE-DB1	Retinal vessel Segmentation	Supervised	CNN	5 layers	-	
Yao *et al.,* [69]	2016	Fundus images	DRIVE	Retinal vessel Segmentation	Supervised	CNN	3 convolutional layers, 3 pooling layers, 1 fully connected layer	Softmax+ local and global binarization	

Dasgupta & Singh [70]	2016	Fundus images	DRIVE	Retinal vessel Segmentation	Supervised	CNN	6 convolutional layers, 1 pooling layer, 1 unsampling layer	Softmax	
Lahiri *et al.,* [12]	2016	Fundus images	DRIVE	Retinal vessel Segmentation	Unsupervised	SDAE	Two parallel SDAE networks	Softmax	
Maninis *et al.,* [71]	2016	Fundus images	DRIVE STARE DRIONS-DB RIM-ONE	Segmentation of OD and retinal vessels	Supervised	CNN	Variation of VGG with last FC layer excluded	-	
Tan *et al.,* [72]	2017	Fundus images	DRIVE	Segmentation of OD, fovea and retinal vessels	Supervised	CNN	6 layers with max pooling	Softmax	
Prentašić & Lončarić [73]	2015	Fundus images	DRiDB	Exudates detection	Supervised	CNN	10 layers with max pooling	Softmax	
Prentašić & Lončarić [74]	2016	Fundus images	DRiDB	Exudates detection	Supervised	CNN	10 layers with max pooling	Softmax	
Shan & Li [75]	2016	Fundus images	DIARETDB	Micro-aneurysm detection	Unsupervised	SSAE	4 layers	Softmax	
Pratt *et al.,* [76]	2016	Fundus images	Kaggle	DR identification	Supervised	CNN	10 convolutional layers, 8 max pooling layers	Softmax	**Retinal Disease Classification**
Abràmoff *et al.,* [77]	2016	Fundus images	MESSIDOR-2	DR Identification	Supervised	CNN based IDx-DR X2.1 system	-	-	
Gulshan *et al.,* [78]	2016	Fundus images	EyePACS-1 MESSIDOR-2	DR detection and classification	Supervised	CNN	Inception-v3 architecture	-	
Colas *et al.,* [79]	2016	Fundus images	Kaggle DR dataset	DR identification	Supervised	DNN	-	-	
Gargeya & Leng [80]	2017	Fundus images	MESSIDOR E-OPHTHA	DR Identification	Supervised	DNN	34 convolutional layers , 1 avg. pooling layer	Softmax	
Burlina *et al.,* [81]	2016	Fundus images	NIH AREDS	AMD detection	Supervised	CNN	-	LSVM	
Burlina *et al.,* [82]	2017	Fundus images	NIH AREDS	AMD detection	Supervised	CNN	-	LSVM	
Lee *et al.,* [83]	2017	OCT images	-	AMD detection	Supervised	CNN	21 layers (VGG16)	-	
Arunkumar & Karthigaikumar [8]	2017	Fundus images	ARIA	Retinal disease Classification	Unsupervised	CNN	GRNN	SVM multi-class	

Melinščak *et al.,* [64] have improved computational efficiency of their deep neural network by using GPU for training of network. Network has four layers of alternating convolutional and max pooling layers with two fully connected layers at the end. Convolutional layers have ReLu activation function and last fully connected layer has Softmax activation function. The DRIVE dataset is used for training of network.

Vessels are extracted from green channel of raw input images i.e. no pre-processing. However, Backpropagation algorithm is used for training of network. The statistical measures obtained after testing of network are shown in Table 4.

Fu *et al.,* [65] have also used probability maps for segmentation of retinal blood vessels. They formulated the problem of vessel extraction as a boundary detection problem. Probability map is constructed by a fully connected four layered CNN with max pooling. Network is a derived form of holistically-nested edge detection (HED) network [84]. Probability maps from all side-output layers are fused together and a single probability map is generated. Instead of sigmoid, rectified linear units (ReLu) are employed in network. The fully connected Conditional Random Fields (CRF) are used for binary segmentation of vessels. The CRF uses probability map and correlation among image pixels to do efficient segmentation. Maximum posterior marginal inference is obtained through mean field approximation of CRF distribution. ARIA dataset is used for fine-tuning of network. Results obtained after examination of algorithm using DRIVE and STARE datasets are presented in Table 4.

Fu *et al.,* [65] presented improved version of their work in reference [66]. Network details are kept same except that CRF is formulated using Recurrent Neural Network (RNN). The network is renamed as DeepVessel network. Training is done following the same footing as presented in old version. Results are depicted in Table 4.

This work has been further extended by Li *et al.,* [68]. Their DNN has five layers with three hidden layers; initially weights of first layer are obtained by pre-training of a de-noising autoencoder. De-noising autoencoder is used to find the relationship between two modalities, image patch and label map. The optimization of network is directly related with this kind of training because naïve learning of weights through backpropagation has high probability of erroneous convergence into local minima. Weights learnt via auto-encoder are employed as initial weights of first layer of deep network and the rest of the weights are randomly initialized. Overall learning and fine tuning of weights is done using backpropagation algorithm. Network is trained with a batch size of 100 and 30 epochs. The probability map, which has the same dimensions as that of original image, is constructed by using label maps obtained from output layer of deep network. Instead of using hessian matrix, vessel segmentation is done via thresholding of probability map. Threshold is chosen so as to increase accuracy. The proposed methodology is tested through ROC analysis using three datasets: DRIVE, STARE, and CHASE-DB1 and results are shown in Table 4. However, methodology is also tested by cross training of network i.e. testing of one dataset on network trained by other two datasets. Accuracy measure decreased from 0.9581, 0.9628, and 0.9527 to 0.9417, 0.9535, and 0.9485 for the CHASE-DB1, STARE and DRIVE datasets when they are trained on DRIVE, CHASE_DB1 and STARE datasets, respectively. Cross training gives an estimate for feasibility criteria of algorithm from clinical point of view.

Yao *et al.,* [69] have used CAFFE architecture[85] for initial segmentation of blood vessels. Their network contains three convolutional layers, three intermediate pooling layers, one fully connected layer and a terminating Softmax classification layer. The preliminary weight selection is done with Gaussian distribution of specified mean and variance whereas further weight learning is done via back-propagation. The output of Softmax layer is confidence level, being blood vessel pixel, with values in the range (0, 1). Classification is perfected by two stage binarization based on three dimensional characteristics of input image; confidence level image from CNN, green channel of RGB retinal input image, and their difference.

The initial binarization is done by global thresholding of image which classifies each pixel as belonging to vessel class or non-vessel class. The local binarization is employed with respect to pixel-class centroid distance. This two stage binarization results in formation of unwanted artifacts which can be removed through morphological post processing i.e. erosion. Structuring elements of varying sizes are used for post processing procedure. Efficacy of algorithm is validated using DRIVE dataset. Results, as shown in Table 4, are comparable to human observer performance measures.

Dasgupta & Singh [70] provided an improved version of supervised structured prediction based multi label method for retinal vessel segmentation. Their CNN has 6 layers including a max pooling layer, an unsampling layer, and a final fully connected Softmax layer. Each convolutional layer has ReLu activation function. Input layer of network is fed with preprocessed green channel extracted image patches. Pre-processing steps include: image normalization, CLAHE, and gamma adjustment. Intensity values are scaled in the range (0, 1). The DRIVE dataset is used for training and testing purposes. This dataset has small number of images therefore; neuron dropout method is used for increasing robustness of network. The results obtained after testing are depicted in Table 4.

Liskowski & Krawiec [67] have compared single pixel classification and structured prediction (SP) based segmentation of vessels. This extensive study is based on different network architectures and pre-processing techniques. Neural Networks can learn features from raw images but pre-processing allows the network to focus on higher order feature extraction. The uneven illumination in input image patches is normalized through global contrast normalization (GCN). Zero phase component analysis (ZCA) is employed for the purpose of single pixel based classification. Neighboring pixels, in normalized image patches, are uncorrelated by multiplication of data matrix with whitening matrix. To increase the number of input samples, normalized and uncorrelated input patches are augmented. Six different types of CNN architectures are developed: PLAIN, GCN, ZCA, AUGMENT, NO-POOL, and BALANCED. As the name suggests NO-POOL network has no intermediate pooling layers, it has four preliminary convolutional layers and four fully connected layers. The PLAIN architecture has two initial convolutional layers followed by a max-pooling layer which is further followed by 2 convolutional layers, one max max-pooling layer and three fully connected layers. GCN, ZCA, AUGMENT architectures are exact replica of PLAIN, they differ in training set-up. For BALANCED network, PLAIN network is trained with equal share of decision classes. Output units have sigmoidal activation whereas hidden layers have ReLu activation units. Results of single pixel based segmentation method for NO-POOL network are verified on DRIVE AND STARE datasets as represented in Table 4.

For structured prediction network architecture, prediction is made for the whole window “s x s” (input image patch). Network is same as that of NO-POOL architecture except that the last layer is replaced by s^2 neurons and is fully connected with the second last layer. This set-up is done for construction of label map. BALANCED and NO-POOL configurations are considered for structural prediction. DRIVE and STARE datasets are used for validation of algorithm; results for NO-POOL structured prediction based network are shown in Table 4.

Structured prediction is more sensitive to false negatives i.e. it is less sensitive to segmentation of fine vessels. On the contrary non structured prediction is reliable for reconstruction of retinal vasculature because it gives less false negative errors.

Table 4 Performance measures for Retinal Vessel landmark detection

Sr. No		Dataset	Learning Method	SN	SP	Acc	AUC	Kappa
1	Wang *et al.,* [61]	DRIVE	Supervised	0.8173	0.9733	0.9767	0.9475	-
		STARE		0.8104	0.9791	0.9813	0.9751	-
2	Melinščak *et al.,* [64]	DRIVE		-	-	0.9466	0.9749	-
3	Fu *et al.,* [65]	DRIVE		0.7294	-	0.9470	-	-
		STARE		0.7140	-	0.9545	-	-
4	Fu *et al.,* [66]	DRIVE		0.7603	-	0.9523	-	-
		STARE		0.7142	-	0.9585	-	-
		CHASE_DB1		0.7130	-	0.9489	-	-
5	Li *et al.,* [68]	DRIVE		0.7569	0.9816	0.9527	0.9738	-
		STARE		0.7726	0.9844	0.9628	0.9879	-
		CHASE-DB1		0.7507	0.9793	0.9581	0.9761	-
6	Yao et al., [69]	DRIVE		0.7731	0.9603	0.9360	-	-
7	Dasgupta & Singh [70]	DRIVE		0.7691	0.9801	0.9533	0.9744	-
8	Liskowski & Krawiec [67]	DRIVE	Supervised without SP	0.7763	0.9768	0.9495	0.9720	0.7781
			Supervised with SP	0.7811	0.9807	0.9535	0.9790	0.7910
		STARE	Supervised without SP	0.7867	0.9754	0.9566	0.9785	0.7622
			Supervised with SP	0.8554	0.9862	0.9729	0.9928	0.8021
9	Lahiri *et al.,* [12]	DRIVE	Unsupervised	-	-	0.9530	-	0.7090
10	Maji *et al.,* [63]	DRIVE	Hybrid	-	-	0.9237	-	0.6287

Simultaneous segmentation of retinal landmarks is also possible through deep learning. Maninis *et al.,* [71] presented the problem of landmark detection as image-image regression problem. They formulated a variation of VGG 16 deep neural network for segmentation of OD and retinal blood vessels. The network is inspired from VGG except that last fully connected (FC) layer is removed. It has 5 stages with multiple convolutional layers and intermediate 4 max pooling layers. Each convolutional layer has ReLu activation unit. Network weights are learned by backpropagation algorithm and stochastic gradient descent. Initial layers of network are efficient in detection of fine features and features become coarser as network proceeds towards output. Therefore, two feature maps are used, one for retinal vessel segmentation and the other for OD segmentation. Datasets are small therefore to increase generalization ability of network; dataset is augmented with rotated and scaled versions of input images. Also, mean is subtracted from each color channel. Efficiency of algorithm towards blood vessel detection is scrutinized using DRIVE and STARE datasets whereas OD segmentation is tested using DRIONS-DB and RIM-ONE dataset. For DRIVE dataset the method achieved 0.822 F1-measure and for stare F1-measure is recorded at 0.831. OD segmentation using DRIONS-DB dataset achieved 0.971 F1-measure while that of RIM-ONE is found to be 0.959. Results are also formulated in Table 5.

Tan *et al.,* [72] have recommended and tested a CNN based deep network for concurrent segmentation of OD, fovea and retinal blood vessels. Three convolution layers with intermediate max pooling layers

constitute the model. Each layer has leaky ReLu activation units. Last fully connected layer has Softmax activation unit. Layer one weights are initialized using Xavier initialization algorithm. Network is trained using backpropagation and stochastic gradient descent. Before any classification input images are normalized using L channel of LUC color space, then images are converted back to RGB color space and green channel is extracted for further processing. Training and testing of network is conducted on DRIVE dataset and Outcomes are articulated in Table 5.

Table 5 Performance measures for simultaneous detection of different retinal landmarks

Sr. No		Dataset	Segmentation	SN	SP	F-score
1	Maninis *et al.,* [71]	DRIVE	Blood Vessels	-	-	0.822
		STARE		-	-	0.831
		DRIONS-DB	OD	-	-	0.971
		RIM-ONE		-	-	0.959
2	Tan *et al.,* [72]	DRIVE	Background	0.9547	0.8063	-
			OD	0.8790	0.9927	-
			Fovea	0.8853	0.9914	-
			Blood Vessels	0.7537	0.9694	-

Exudates, lipids and lipoproteins are pre-eminent signs of DR. The exudates are of varying sizes, they can vary from very small size to the size as large as that of an OD. Deep neural networks provide a worthwhile arrangement for detection of exudates in retinal fundus images. This technique has been followed by Prentašić & Lončarić [73] in their study for automatic detection of exudates. Network is fed with green plane of RGB retinal image. OD is the less potential area in retina for detection of exudates therefore OD is detected and masked using HIS component of image. DRiDB data is used for training and testing of deep network. Table 6 shows the results obtained after testing.

Prentašić & Lončarić [74] extended their work and presented a novel approach of combining probability maps from CNN with other landmark detection probability maps. This approach is used to exploit the domain knowledge that exudates don't appear inside retinal blood vessels and OD. Deep network has the same setting as described in their previous work [73]. Probability maps from OD detection, retinal vessel detection, and parabola fitting are combined to give one probability map which is then combined with output of CNN. The OD detection probability map is obtained from an ensemble of strategies which include: entropy based approach [86], Laplacian of Gaussian approach, brightness approach [87], and Hough transformation method. Unevenly illuminated fundus images have bright borders which may result in detection of false positives. Therefore, an estimated border is subtracted form green channel of image to get rid of bright borders. Blood vessel probability map is generated by using Farangi vesselness filter [88]. After blood vessel and OD detection a parabola is fitted at the center of OD which encapsulates the regions where there is less potential of exudate presence. The CNN is trained and tested with DRiDB dataset. At the time of training, input image is de-noised using total variation (TV) regularization de-noising. Probability map obtained by last Softmax activation function layer is combined with landmark detection probability map and exudates are detected. Results are formulated in Table 6.

Table 6 Performance measures for detection of exudates

Sr. No		Dataset	SN	PPV	F-score
1	Prentašić & Lončarić [73]	DRiDB	0.77	0.77	0.77
2	Prentašić & Lončarić [74]	DRiDB	0.78	0.78	0.78

4.1.2 Hybrid Method

Hybrid DNN is constructed using an unsupervised training followed by supervised classifier training. Maji *et al.,* [63] have followed this technique for retinal vessel segmentation. They have used two DAEs followed by an RF classifier for extraction of vessels. The unsupervised pre-training of stacked auto-encoder is used for learning weights of network. Once pre-training is done, an ensemble RF classifier is trained in a supervised manner in the presence of ground truth and algorithm is tested on DRIVE dataset. The maximum accuracy obtained with a Kappa coefficient (0.6287) is 0.9237 as depicted in Table 4. The results obtained are not good compared to traditional methods but they give a state-of-the-art for hybrid DNNs.

4.1.3 Unsupervised Methods

Retinal vessel segmentation can also be done using unsupervised deep learning methods, although this field is not that much explored but it has the potential to surpass statistical measures obtained from current state-of-the-art methods.

Lahiri *et al.,* [12] has presented a two level stacked de-noised auto-encoder (SDAE) network for retinal vessel segmentation. In order to get the best contrast of vessels with background, green plane of RGB image is extracted. Contrast limited adaptive histogram equalization (CLAHE) is employed to get rid of uneven illumination. Vessel and background patches of image, for training of de-noised auto-encoder (DAE), are obtained through sampling of a manually annotated vasculature. Redundant foreground pixel sampling is avoided through skeletonization. Efficient segregation of vessel and background pixels is obtained by sampling background pixels from a dilated image. Diversification is added by feeding DAE with alternate vessel and background patches. A simple DAE has three layers with one hidden layer. Random noise is deliberately added in the input to achieve unsupervised learning. The backpropagation is exploited to minimize loss function and weight matrix is updated using L-BFG (Limited Memory Broyden-Fletcher-Goldfarb-Shanno). Stacked DAE is obtained by taking hidden layer output of first DAE as input to second DAE and training it. After this training the last output layer is replaced with a single node Softmax classifier. The first level of ensemble is formed by making a collection of *n* DAEs termed as E1.net. Multiple DAE kernels allow the vessel feature learning in multiple directions. An SDAE (2 hidden layers) with Softmax classified output makes the second level of ensemble. Further diversification is added by parallel training of two E1.nets with different architecture. Convex weighted average is used to get the combined decision of both E1.nets. The algorithm is tested using publically available DRIVE dataset. The maximum average accuracy is recorded at 0.953 and Kappa agreement coefficient at 0.709 as presented in Table 4. This method outperformed the human observer accuracy which was recorded at 0.947.

Micro-aneurysms (MA) rupture retinal blood vessels and make blood to leak from them. These miniature lesions appear as early signs of DR, therefore they play a pivotal role in timely detection of DR. Automatic extraction of these lesions from 2-D fundus images has been demonstrated by Shan & Li [75]. There is no need to extract blood vessels from images. Extraction of MA features is done straightaway from raw image patches. Image patches are segregated into two classes i.e. lesion present and non-lesion present. Sampling of image patches is done from green channel of input image. Before sampling, pixel values are adjusted so that they lie in the range (0, 1). Computer-aided feature extraction is done with the help of stacked sparse auto-encoder (SSAE) and Softmax classifier is used to label features. Two hidden layers

constitute SSAE. First layer is used to extract features from raw image patches and second layer learns intricate features from output of first layer. Softmax binary classifier is connected with second layer of SSAE. Algorithm is scrutinized with the help of DIARETDB dataset. Classification results from Softmax classifier are tuned by varying patch-sizes. Fine tuning has provided steady state and more efficient results as compared to previous ones. Results, as depicted in Table 7, are classified on the basis of tuning.

Table 7 Performance measures for detection of micro-aneurysms using DIARET-DB dataset

	Dataset	Tuning	Precision	Recall	SP	F-score	Acc	AUC
Shan & Li [75]	DIARET-DB	Before	0.8850	0.8652	0.8873	0.8742	0.8762	0.9341
		After	0.9157	0.9116	0.9160	0.9134	0.9138	0.9620

4.2 Retinal Disease Classification

4.2.1 Supervised Methods

Distinctive characterization of retinal diseases requires experienced clinicians but the advancement in the fields of image processing and machine learning helped in completely automating this process. As the traditional methods for classification of retinal diseases reached excellence, advent of deep learning has provided afresh way for efficient and accurate diagnosis of retinal diseases.

An automated screening algorithm for classification of DR into severe, proliferative, and non-proliferative is recommended by Colas et al., [79]. They developed a deep learning based neural network. The algorithm is tested using Kaggle DR Detection challenge dataset. This dataset has 10,000 images captured from 5000 patients. The algorithm achieved an AUC of 0.946, sensitivity of 0.962, and 0.666 specificity as shown in Table 8.

Pratt et al., [76] proposed a method for identification and classification of DR into four categories: mild DR, moderate DR, severe DR, and proliferative DR. Deep network extracts features form retinal image which are required for classification of DR. It consists of ten convolutional layers with intermediate max pooling layers followed by two fully connected and a Softmax classification layer. Each layer has leaky ReLu activation unit and L2 normalization for weights and biases. Color normalization, using OpenCV package, is done to even out unnecessary variations in input images. Gaussian initialized weights are batch normalized after each layer. To avoid over fitting, weighted class weights and node dropout strategy is used. Network is trained through stochastic gradient descent and Nestrov momentum weight learning methods. After pre-training, network is further trained with real time augmented image patches. This is done to improve localization ability of system. Legitimacy of algorithm is tested on Kaggle dataset. Proposed method provided 95% sensitivity and 75% accuracy as presented in Table 8.

Abràmoff *et al.,* [77] provided an improved version of their algorithm for classification of DR and ME, older version of algorithm was developed without incorporating deep learning. New algorithm provides automatic identification and Classification of DR into moderate, severe non proliferative DR (NPDR), proliferative DR (PDR), and ME with improved statistical measures. They used IDX-DR version X2.1 automated system. The device was trained using EyeCheck project dataset. Evaluation of system is done using Messidor-2 dataset. The findings are presented in Table 8.

A method for identification of DR and diabetic is presented by Gulshan *et al.,* [78]. They used Inception v3 deep neural network architecture [89]. EyePACS-1 and MESSIDOR-2 datasets are used for training and testing of network. ImageNet dataset is used for initialization of network weights. The weights are learned via distributed stochastic gradient and training of network is made efficient by using batch normalization. Algorithm is inspected using two operating points. Focus of first operating point is high specificity and that of second is high sensitivity. Results obtained are shown in Table 8.

Clinician could be aided in grading of DR through a visualization heatmap. Gargeya & Leng [80] have provided an automated convolutional neural network based model for grading of DR and they also generated heatmap for easy abnormality detection by clinicians. Network has convolutional blocks with 4, 6, 8, and 10 layers. Each layer incorporates batch normalization and ReLu activation units. Last layer is Softmax classification layer preceded by an average pooling layer and a visualization layer. Heatmap is generated using visualization layer which has functionality similar to that of a convolutional layer. Training of model is done on EyePACS dataset. Input images are normalized, downsized and augmented to reduce the unnecessary varying brightness and contrast. Some meta-data, related to original image, is appended with feature vector to normalize the effect of environmental variables. Algorithm provided 0.97 AUC, with 0.94 and 0.98 sensitivity and specificity respectively for EyePACS dataset. Generalization ability of algorithm is tested using MESSIDOR-2 and E-OPTHA datasets. Results are presented in Table 8.

Table 8 Performance measures for grading DR severity

Sr. No		Dataset	SN	SP	Acc	AUC
1	Colas *et al.,* [79]	From Kaggle competition	0.962	0.666	-	0.9460
2	Pratt *et al.,* [76]	From Kaggle competition	0.950	-	0.750	-
3	Abràmoff *et al.,* [77]	MESSIDOR-2	0.968	0.87	-	0.980
4	Gulshan *et al.,* [78]	EYE-PACS1	0.975	0.934	-	-
		MESSIDOR-2	0.961	0.939	-	-
5	Gargeya & Leng [80]	MESSIDOR 2	0.93	0.87	-	0.94
		E-OPTHA	0.90	0.94	-	0.95

Identification of Age Related Macular Degeneration (AMD) is a crucial task. Silent nature of the disease, during intermediate stage, results in asymptotic severity leading to complete vision loss. Features learnt from pre-trained neural networks can help in effective diagnosis of AMD at intermediate stage. Burlina *et al.,* [81] have checked appropriateness of this technique for classification of AMD. Overfeat Features (OF) are extracted from pre-trained deep convolutional neural network (DCNN) on a generic dataset ImageNet. Resized images are fed into DCNN for learning OF features. Most imperative prognostic retinal image area for AMD diagnosis is the central part of retina. This information is utilized by extracting features appended from multiple concentric square grids. Linear Support Vector Machine (LSVM) is trained with extracted features. Efficiency of model is scrutinized using NIH AREDS dataset. The dataset is divided into two classes i.e. EIPC (equal number of images per class) and MIPC (maximum number of images per class). Performance is evaluated on both classes of dataset as presented in Table 9.

Burlina *et al.,* [82] have provided a comparison of disease prediction between human and algorithm. Classification problem is divided into four categories. Class 1 corresponds to no AMD, class 2 incorporates

early stage AMD cases, class 3 encompasses intermediate stage AMD, and class 4 denotes advanced form of AMD. The Comparison shows that algorithm's results are in close proximity to those of physician as depicted in Table 9..

3D optical coherence tomography (OCT) imaging modality is the most common among imaging modalities in the field of ophthalmology. OCT images combined with electronic medical records (EMR) give a rich dataset for training of deep neural networks. Lee *et al.,* [83] have followed the same footings for AMD detection. They implemented Vgg16 deep neural network for efficient classification of AMD using OCT images. Network consists of 21 layers, including convolutional layers and max pooling layers, each with a ReLu activation unit. Automatically extracted OCT images are used for training and testing of network. Weights are initialized using Xavier algorithm and optimized by stochastic gradient descent. Input images are first downsized and histogram equalized and then fed into network. Results are shown in Table 9.

Table 9 Performance measures for grading AMD severity

Sr. No		Dataset	AMD Class	SN	SP	Acc	AUC	Kappa
1	Burlina *et al.,* [81]	EIPC	-	0.942-0.964	0.899-0.920	0.921-0.942	-	-
		MIPC	-	0.909-0.957	0.901-0.956	0.919-0.950	-	-
2	Burlina *et al.,* [82]	NIH AREDS	4	-	-	0.794	-	0.6962
			3	-	-	0.815	-	0.7226
			2	-	-	0.934	-	0.8482
3	Lee *et al.,* [83]	3D OCT Images	-	0.9264	0.9369	0.9345	0.9745	-

4.2.2 Unsupervised Methods

Unsupervised Deep neural networks have proved effective for classification of retinal diseases such as: AMD and DR. This approach has been suggested by Arunkumar & Karthigaikumar [8]. Generalized regression neural network (GRNN) is used for reduction of feature vector dimension. This is done to improve compute time efficiency. Model is able to extract intricate features because it includes stacked Restricted Boltzman Machine (RBM) in its layers. Input images are first preprocessed to remove noise and adjust contrast. Effectiveness of system is checked on ARIA dataset. Results are recorded in Table 10.

Table 10 Performance measures for classification of different retinal diseases

	Dataset	SN	SP	Acc
Arunkumar & Karthigaikumar [8]	ARIA	0.7932	0.9789	0.8762

5 Discussion

Supervised learning approach is better compared to unsupervised approach because network learns the mapping efficiently due to presence of ground truth data. This can also be observed from all performance measures recorded in the above section. Most of the progress in deep learning based retinal image analysis has been witnessed in segmentation of retinal vasculature. Among all the DNN based algorithms which utilize intensity level pixel information, Li *et al.,* [68] have provided the maximum AUC of 0.9879. However, use of only intensity level information undermines the efficiency of algorithm because

neighboring pixels always have a certain correlation factor. The blood vessel segmentation methodology proposed by Liskowski & Krawiec [67] has provided the best performance metrics. As they utilized contextual information along with intensity level information of pixels therefore their model outperformed other retinal blood vessel segmentation techniques. It achieved maximum AUC of 0.9928 which is higher than best to date AUC recorded by other traditional approaches. Instead of following a tedious approach i.e. one by one retinal landmark detection, DNNs can be used for simultaneous extraction of retinal landmarks from retinal images. This approach is presented by Tan *et al.,* [72]. DNN have not yet been much explored for retinal pathology detection. Prentašić & Lončarić [74] have provided state-of-the-art results for detection of exudates. The method proposed by Shan & Li [75] for micro-aneurysm detection through SSAE achieved an AUC of 0.9620. DNN is still an underexplored technique in the field of retinal pathology detection. Lee *et al.,* [83] have proved efficacy of DNN for grading of AMD in 3D OCT images by recording an AUC of 0.9745. Supervised DNN approach have also been employed for efficient grading of DR. Colas *et al.,* [79], Pratt *et al.,* [76], Gulshan *et al.,* [78], Gargeya & Leng [80] are examples of this effort. Among all of them, Abràmoff *et al.,* [77] have achieved the maximum AUC of 0.980 for grading of DR.

6 Conclusion

Automated extraction and classification of retinal pathology is an active research area, which is now employed in practice for many ophthalmologic screening tests [90]. The retinal image analysis through deep neural networks is a nascent field. Although research has been conducted in extraction of retinal landmarks and pathologies but epitome of this technique is yet to be witnessed. Moreover, unsupervised learning based DNNs have not seen much progress. Deep learning techniques can be efficiently applied for segmentation of dot and blot hemorrhages, cotton wool spots, hard exudates, soft exudates, drusen etc. There is no restriction on number of layers and architecture of neural network, network architecture is chosen heuristically in accordance with problem domain. The variants of Deep Neural Networks like AlexNet, LSTM, VggNet, and GoogleNet can be used for extraction of retinal anatomical structures. Although Vgg-16 is used by Lee *et al.,* [83] for 3D OCT retinal image analysis; however, there is no precedence of its use in case of color fundus images. All these networks are very deep and they have capability of extracting much more complex features than those extracted by traditional methods and with better performance measures. This property makes DNN capable of replacing traditional ophthalmologic screening practices.

REFERENCES

[1] Fraz, M.M., et al., *Blood vessel segmentation methodologies in retinal images–a survey.* Computer methods and programs in biomedicine, 2012. **108**(1): p. 407-433.

[2] Abràmoff, M.D., M.K. Garvin, and M. Sonka, *Retinal imaging and image analysis.* IEEE reviews in biomedical engineering, 2010. **3**: p. 169-208.

[3] Abdullah, M. and M.M. Fraz. *Application of grow cut algorithm for localization and extraction of optic disc in retinal images*. in *2015 12th International Conference on High-capacity Optical Networks and Enabling/Emerging Technologies (HONET)*. 2015. IEEE.

[4] Fraz, M.M., et al. *Automated Arteriole and Venule Recognition in Retinal Images using Ensemble Classification*. in *9th International Conference on Computer Vision Theory and Applications (VISAAP)*. 2014. Lisbon, Portugal.

[5] Fraz, M., et al., *Computational methods for exudates detection and macular edema estimation in retinal images: a survey.* Archives of Computational Methods in Engineering, 2018: p. 1-28.

[6] Fraz, M.M., et al., *Multiscale segmentation of exudates in retinal images using contextual cues and ensemble classification.* Biomedical Signal Processing and Control, 2017. **35**: p. 50-62.

[7] Basit, A. and M.M. Fraz, *Optic disc detection and boundary extraction in retinal images.* Applied Optics, 2015. **54**(11): p. 3440-3447.

[8] Arunkumar, R. and P. Karthigaikumar, *Multi-retinal disease classification by reduced deep learning features.* Neural Computing and Applications, 2017. **28**(2): p. 329-334.

[9] Sidibé, D., I. Sadek, and F. Mériaudeau, *Discrimination of retinal images containing bright lesions using sparse coded features and SVM.* Computers in biology and medicine, 2015. **62**: p. 175-184.

[10] Sadek, I., D. Sidibé, and F. Meriaudeau. *Automatic discrimination of color retinal images using the bag of words approach*. in *SPIE Medical Imaging*. 2015. International Society for Optics and Photonics.

[11] Veras, R., et al. *SURF descriptor and pattern recognition techniques in automatic identification of pathological retinas*. in *Intelligent Systems (BRACIS), 2015 Brazilian Conference on*. 2015. IEEE.

[12] Lahiri, A., et al. *Deep neural ensemble for retinal vessel segmentation in fundus images towards achieving label-free angiography*. in *Engineering in Medicine and Biology Society (EMBC), 2016 IEEE 38th Annual International Conference of the*. 2016. IEEE.

[13] Badar, M., M. Shahzad, and M.M. Fraz. *Simultaneous Segmentation of Multiple Retinal Pathologies Using Fully Convolutional Deep Neural Network*. 2018. Cham: Springer International Publishing.

[14] Zahoor, M.N. and M.M. Fraz, *Fast Optic Disc Segmentation in Retina Using Polar Transform.* IEEE Access, 2017. **5**: p. 7.

[15] Patton, N., et al., *Retinal image analysis: concepts, applications and potential.* Progress in retinal and eye research, 2006. **25**(1): p. 99-127.

[16] Albert, D.M. and W.H. Miller, *Jan Purkinje and the ophthalmoscope.* American journal of ophthalmology, 1973. **76**(4): p. 494-499.

[17] Fraz, M.M., et al., *QUARTZ: Quantitative Analysis of Retinal Vessel Topology and size – An automated system for quantification of retinal vessels morphology.* Expert Systems with Applications, 2015. **42**(20): p. 7221-7234.

[18] Huang, D., et al., *Optical coherence tomography.* Science (New York, NY), 1991. **254**(5035): p. 1178.

[19] Bennett, T.J. and C.J. Barry, *Ophthalmic imaging today: an ophthalmic photographer's viewpoint–a review.* Clinical & experimental ophthalmology, 2009. **37**(1): p. 2-13.

[20] Venkatesh, P., et al., *Detection of retinal lesions in diabetic retinopathy: comparative evaluation of 7-field digital color photography versus red-free photography.* International ophthalmology, 2015. **35**(5): p. 635-640.

[21] Tyler, M.E., *Stereo fundus photography: Principles and technique.* J Ophthalmic Photogr, 1996. **18**(2): p. 6-81.

[22] Hirohara, Y., et al., *Validity of retinal oxygen saturation analysis: Hyperspectral imaging in visible wavelength with fundus camera and liquid crystal wavelength tunable filter.* Optical review, 2007. **14**(3): p. 151.

[23] Alabboud, I., et al. *New spectral imaging techniques for blood oximetry in the retina*. in *European Conference on Biomedical Optics*. 2007. Optical Society of America.

[24] Webb, R.H. and G.W. Hughes, *Scanning laser ophthalmoscope.* IEEE Transactions on Biomedical Engineering, 1981(7): p. 488-492.

[25] Roorda, A., et al., *Adaptive optics scanning laser ophthalmoscopy.* Optics express, 2002. **10**(9): p. 405-412.

[26] Ng, E., et al., *Ophthalmological Imaging and Applications*. 2014: CRC Press.

[27] Slakter, J.S., et al., *Indocyanine-green angiography.* Current opinion in ophthalmology, 1995. **6**(3): p. 25-32.

[28] Niemeijer, M., et al., *DRIVE: digital retinal images for vessel extraction.* Methods for Evaluating Segmentation and Indexing Techniques Dedicated to Retinal Ophthalmology, 2004.

[29] Hoover, A., V. Kouznetsova, and M. Goldbaum, *Locating blood vessels in retinal images by piecewise threshold probing of a matched filter response.* IEEE Transactions on Medical imaging, 2000. **19**(3): p. 203-210.

[30] *ARIA Online, Retinal Image Archivehttp://www.eyecharity.com/aria online/, 2006.*

[31] Fraz, M.M., et al., *An Ensemble Classification-Based Approach Applied to Retinal Blood Vessel Segmentation.* IEEE Transactions on Biomedical Engineering, 2012. **59**(9): p. 2538-2548.

[32] Quellec, G., et al., *Optimal wavelet transform for the detection of microaneurysms in retina photographs.* IEEE Transactions on Medical Imaging, 2008. **27**(9): p. 1230-1241.

[33] Decencière, E., et al., *Feedback on a publicly distributed image database: the Messidor database.* Image Analysis & Stereology, 2014. **33**(3): p. 231-234.

[34] Decencière, E., et al., *TeleOphta: Machine learning and image processing methods for teleophthalmology.* Irbm, 2013. **34**(2): p. 196-203.

[35] Prentašić, P., et al. *Diabetic retinopathy image database(DRiDB): A new database for diabetic retinopathy screening programs research*. in *2013 8th International Symposium on Image and Signal Processing and Analysis (ISPA)*. 2013.

[36] Drexler, W. and J.G. Fujimoto, *Optical coherence tomography: technology and applications*. 2015: Springer.

[37] Jakobiec, F.A., *Ocular anatomy, embryology, and teratology*. 1982: Harpercollins.

[38] Welikala, R.A., et al., *Automated retinal image quality assessment on the UK Biobank dataset for epidemiological studies.* Computers in biology and medicine, 2016. **71**: p. 67-76.

[39] Owen, C.G., et al., *Retinal Vasculometry Associations with Cardiometabolic Risk Factors in the European Prospective Investigation of Cancer—Norfolk Study.* Ophthalmology, 2018.

[40] Beagley, J., et al., *Global estimates of undiagnosed diabetes in adults.* Diabetes research and clinical practice, 2014. **103**(2): p. 150-160.

[41] Raman, V., P. Then, and P. Sumari. *Proposed retinal abnormality detection and classification approach: Computer aided detection for diabetic retinopathy by machine learning approaches*. in *Communication Software and Networks (ICCSN), 2016 8th IEEE International Conference on*. 2016. IEEE.

[42] Welikala, R.A., et al., *Genetic algorithm based feature selection combined with dual classification for the automated detection of proliferative diabetic retinopathy.* Computerized Medical Imaging and Graphics, 2015. **43**(0): p. 64-77.

[43] Engerman, R.L., *Pathogenesis of diabetic retinopathy.* Diabetes, 1989. **38**(10): p. 1203-1206.

[44] Kowluru, R.A. and P.-S. Chan, *Capillary dropout in diabetic retinopathy*, in *Diabetic Retinopathy*. 2008, Springer. p. 265-282.

[45] Kanski, J.J. and B. Bowling, *Clinical ophthalmology: a systematic approach*. 2011: Elsevier Health Sciences.

[46] Klein, R., et al., *The Wisconsin Epidemiologic Study of Diabetic Retinopathy XXIII: the twenty-five-year incidence of macular edema in persons with type 1 diabetes.* Ophthalmology, 2009. **116**(3): p. 497-503.

[47] Varma, R., et al., *Prevalence of and risk factors for diabetic macular edema in the United States.* JAMA ophthalmology, 2014. **132**(11): p. 1334-1340.

[48] Jager, R.D., W.F. Mieler, and J.W. Miller, *Age-related macular degeneration.* New England Journal of Medicine, 2008. **358**(24): p. 2606-2617.

[49] Alfaro, D.V., *Age-related macular degeneration: a comprehensive textbook*. 2006: Lippincott Williams & Wilkins.

[50] Fraz, M.M., et al. *Retinal vessel segmentation using ensemble classifier of bagged decision trees*. in *IET Conference Publications*. 2012. IEE.

[51] Fraz, M.M., et al., *Delineation of blood vessels in pediatric retinal images using decision trees-based ensemble classification.* International Journal of Computer Assisted Radiology and Surgery, 2014. **9**(5): p. 795-811.

[52] Liew, G. and J.J. Wang, *Retinal vascular signs: a window to the heart?* Revista Española de Cardiología (English Edition), 2011. **64**(6): p. 515-521.

[53] Quigley, H.A. and A.T. Broman, *The number of people with glaucoma worldwide in 2010 and 2020.* British journal of ophthalmology, 2006. **90**(3): p. 262-267.

[54] Zahoor, M.N. and M.M. Fraz, *A Correction to the Article "Fast Optic Disc Segmentation in Retina Using Polar Transform".* IEEE Access, 2018. **6**: p. 4845-4849.

[55] Fraz, M.M., et al., *Delineation of blood vessels in pediatric retinal images using decision trees-based ensemble classification.* International Journal of Computer Assisted Radiology and Surgery, 2014. **9**(5): p. 795-811.

[56] Thomas, R. and R.S. Parikh, *How to assess a patient for glaucoma.* Community eye health, 2006. **19**(59): p. 36.

[57] Goodfellow, I., Y. Bengio, and A. Courville, *Deep learning*. 2016: MIT press.

[58] Hsu, F.-H., *Behind Deep Blue: Building the computer that defeated the world chess champion*. 2002: Princeton University Press.

[59] LeCun, Y., Y. Bengio, and G. Hinton, *Deep learning.* Nature, 2015. **521**(7553): p. 436-444.

[60] Angelov, P. and A. Sperduti. *Challenges in deep learning*. in *Proceedings of the 24th European symposium on artificial neural networks (ESANN)*. 2016.

[61] Wang, S., et al., *Hierarchical retinal blood vessel segmentation based on feature and ensemble learning.* Neurocomputing, 2015. **149**: p. 708-717.

[62] Fang, T., et al. *Retinal vessel landmark detection using deep learning and hessian matrix*. in *Image and Signal Processing (CISP), 2015 8th International Congress on*. 2015. IEEE.

[63] Maji, D., et al. *Deep neural network and random forest hybrid architecture for learning to detect retinal vessels in fundus images*. in *Engineering in Medicine and Biology Society (EMBC), 2015 37th Annual International Conference of the IEEE*. 2015. IEEE.

[64] Melinščak, M., P. Prentašić, and S. Lončarić. *Retinal vessel segmentation using deep neural networks*. in *VISAPP 2015 (10th International Conference on Computer Vision Theory and Applications)*. 2015.

[65] Fu, H., et al. *Retinal vessel segmentation via deep learning network and fully-connected conditional random fields*. in *Biomedical Imaging (ISBI), 2016 IEEE 13th International Symposium on*. 2016. IEEE.

[66] Fu, H., et al. *DeepVessel: Retinal Vessel Segmentation via Deep Learning and Conditional Random Field*. in *International Conference on Medical Image Computing and Computer-Assisted Intervention*. 2016. Springer.

[67] Liskowski, P. and K. Krawiec, *Segmenting Retinal Blood Vessels With<? Pub_newline?> Deep Neural Networks.* IEEE transactions on medical imaging, 2016. **35**(11): p. 2369-2380.

[68] Li, Q., et al., *A cross-modality learning approach for vessel segmentation in retinal images.* IEEE transactions on medical imaging, 2016. **35**(1): p. 109-118.

[69] Yao, Z., Z. Zhang, and L.-Q. Xu. *Convolutional Neural Network for Retinal Blood Vessel Segmentation*. in *Computational Intelligence and Design (ISCID), 2016 9th International Symposium on*. 2016. IEEE.

[70] Dasgupta, A. and S. Singh, *A Fully Convolutional Neural Network based Structured Prediction Approach Towards the Retinal Vessel Segmentation.* arXiv preprint arXiv:1611.02064, 2016.

[71] Maninis, K.-K., et al. *Deep retinal image understanding*. in *International Conference on Medical Image Computing and Computer-Assisted Intervention*. 2016. Springer.

[72] Tan, J.H., et al., *Segmentation of optic disc, fovea and retinal vasculature using a single convolutional neural network.* Journal of Computational Science, 2017.

[73] Prentašić, P. and S. Lončarić. *Detection of exudates in fundus photographs using convolutional neural networks*. in *Image and Signal Processing and Analysis (ISPA), 2015 9th International Symposium on*. 2015. IEEE.

[74] Prentašić, P. and S. Lončarić, *Detection of exudates in fundus photographs using deep neural networks and anatomical landmark detection fusion.* Computer Methods and Programs in Biomedicine, 2016. **137**: p. 281-292.

[75] Shan, J. and L. Li. *A Deep Learning Method for Microaneurysm Detection in Fundus Images*. in *Connected Health: Applications, Systems and Engineering Technologies (CHASE), 2016 IEEE First International Conference on*. 2016. IEEE.

[76] Pratt, H., et al., *Convolutional Neural Networks for Diabetic Retinopathy.* Procedia Computer Science, 2016. **90**: p. 200-205.

[77] Abràmoff, M.D., et al., *Improved Automated Detection of Diabetic Retinopathy on a Publicly Available Dataset Through Integration of Deep LearningDeep Learning Detection of Diabetic Retinopathy.* Investigative Ophthalmology & Visual Science, 2016. **57**(13): p. 5200-5206.

[78] Gulshan, V., et al., *Development and validation of a deep learning algorithm for detection of diabetic retinopathy in retinal fundus photographs.* JAMA, 2016. **316**(22): p. 2402-2410.

[79] Colas, E., et al., *Deep learning approach for diabetic retinopathy screening.* Acta Ophthalmologica, 2016. **94**(S256).

[80] Gargeya, R. and T. Leng, *Automated Identification of Diabetic Retinopathy Using Deep Learning.* Ophthalmology, 2017.

[81] Burlina, P., et al. *Detection of age-related macular degeneration via deep learning*. in *Biomedical Imaging (ISBI), 2016 IEEE 13th International Symposium on*. 2016. IEEE.

[82] Burlina, P., et al., *Comparing humans and deep learning performance for grading AMD: A study in using universal deep features and transfer learning for automated AMD analysis.* Computers in Biology and Medicine, 2017. **82**: p. 80-86.

[83] Lee, C.S., D.M. Baughman, and A.Y. Lee, *Deep Learning Is Effective for Classifying Normal versus Age-Related Macular Degeneration Optical Coherence Tomography Images.* Ophthalmology Retina, 2017.

[84] Xie, S. and Z. Tu. *Holistically-nested edge detection*. in *Proceedings of the IEEE International Conference on Computer Vision*. 2015.

[85] Jia, Y., et al. *Caffe: Convolutional architecture for fast feature embedding*. in *Proceedings of the 22nd ACM international conference on Multimedia*. 2014. ACM.

[86] Sopharak, A., et al., *Automatic detection of diabetic retinopathy exudates from non-dilated retinal images using mathematical morphology methods.* Computerized medical imaging and graphics, 2008. **32**(8): p. 720-727.

[87] Walter, T. and J.-C. Klein. *Segmentation of color fundus images of the human retina: Detection of the optic disc and the vascular tree using morphological techniques*. in *International Symposium on Medical Data Analysis*. 2001. Springer.

[88] Frangi, A.F., et al. *Multiscale vessel enhancement filtering*. in *International Conference on Medical Image Computing and Computer-Assisted Intervention*. 1998. Springer.

[89] Szegedy, C., et al. *Rethinking the inception architecture for computer vision*. in *Proceedings of the IEEE Conference on Computer Vision and Pattern Recognition*. 2016.

[90] Badawi, S.A. and M.M. Fraz, *Optimizing the trainable B-COSFIRE filter for retinal blood vessel segmentation.* PeerJ, 2018. **6**: p. e5855.

